

HiZELS: the High Redshift Emission Line Survey with UKIRT

*Philip Best¹, Ian Smail², David Sobral¹, Jim Geach², Timothy Garn¹, Rob Ivison³
Jaron Kurk⁴, Gavin Dalton^{5,6}, Michele Cirasuolo^{1,2}, Mark Casali⁷*

1: SUPA, Institute for Astronomy, Royal Observatory, Blackford Hill, Edinburgh, EH9 3HJ, UK

2: Institute of Computational Cosmology, Durham University, South Road, Durham, DH1 3LE, UK

3: Astronomy Technology Centre, Royal Observatory, Blackford Hill, Edinburgh, EH9 3HJ, UK

4: Max-Planck-Institut für Astronomie, Königstuhl, 17 D-69117, Heidelberg, Germany

5: Astrophysics, Department of Physics, Keble Road, Oxford, OX1 3RH, UK

6: Space Science and Technology, Rutherford Appleton Laboratory, HSIC, Didcot, OX11 0QX, UK

7: European Southern Observatory, Karl-Schwarzschild-Strasse 2, D-85738 Garching, Germany

Abstract: In these proceedings we report on HiZELS, the High-z Emission Line Survey, our successful panoramic narrow-band Campaign Survey using WFCAM on UKIRT to detect and study emission line galaxies at $z \simeq 1-9$. HiZELS employs the H₂(S1) narrow-band filter together with custom-made narrow-band filters in the *J* and *H*-bands, with the primary aim of delivering large identically-selected samples of H α emitting galaxies at redshifts of 0.84, 1.47 and 2.23. Comparisons between the luminosity function, the host galaxy properties, the clustering, and the variation with environment of these H α -selected samples are yielding unique constraints on the nature and evolution of star-forming galaxies, across the peak epoch of star-formation activity in the Universe. We provide a summary of the project status, and detail the main scientific results obtained so far: the measurement of the evolution of the cosmic star-formation rate density out to $z > 2$ using a single star-formation indicator, determination of the morphologies, environments and dust-content of the star-forming galaxies, and a detailed investigation of the evolution of their clustering properties. We also summarise the on-going work and future goals of the project.

1. Introduction

The fundamental observables required to understand the basic features of galaxy formation and evolution are the volume-averaged star-formation rate as a function of epoch, its distribution function within the galaxy population, and the variation with environment. Surveys of the star-formation rate as a function of epoch suggest that the star-formation rate density rises as $\sim (1+z)^4$ out to at least $z \sim 1$ (e.g. Lilly et al. 1996), and then flattens, with the bulk of stars seen in galaxies today having been formed between $z \sim 1-3$. Determining the precise redshift where the star-formation rate peaked is more difficult, however, with different star-formation indicators giving widely different measures of the integrated star-formation rate density (see Hopkins et al. 2006). These problems are exacerbated by the effects of cosmic variance in the current samples, which are typically based on small-field surveys.

The H α emission line is a very well-calibrated measure of star-formation rate in the nearby Universe (e.g. Kennicutt 1998; Moustakas et al. 2006). As it redshifts through the optical and near-IR bands, it offers a single star-formation indicator which can be studied from $z = 0$ to $z \sim 3$, right through the peak star-formation epoch in the Universe. It is relatively immune to dust extinction, and has sufficient sensitivity that estimates of the integrated star-formation rate don't require large extrapolations for faint sources below the sensitivity limit: surveys with a sensitivity of $\sim 10 M_{\odot} \text{ yr}^{-1}$ can be undertaken in H α at $z \sim 2$ with current instrumentation, compared to limits of $\sim 10^2-10^3 M_{\odot} \text{ yr}^{-1}$ for other dust-independent tracers such as radio, far-infrared and sub-mm luminosities (e.g. Ivison et al. 2007).

The $H\alpha$ emission line has been widely used as a method of tracing the evolution of star-formation, both through spectroscopic surveys and via imaging surveys exploiting narrow-band filters (e.g. Gallego et al. 1995; Yan et al. 1999; Tresse et al. 2002; Doherty et al. 2006). Narrow-band surveys offer a sensitive and unbiased method of detecting emission-line objects lying in large well-defined volumes; the sources are identified on the strength of their emission line and thus crudely represent a star-formation rate-selected sample, and they must lie in a narrow range in redshift. Before the advent of large-area near-IR detectors such as WFCAM, narrow-band $H\alpha$ surveys in the near-IR (i.e. at $z \gtrsim 0.7$) were limited to very small areas and sample sizes (the largest at $z \sim 2$ had just ~ 10 candidate sources; Moorwood et al. 2000). The primary goal of HiZELS is to overcome this, with wide-area surveys using narrow-band filters in the J , H and K -bands to detect of order a thousand star-forming galaxies in $H\alpha$ at each of three redshifts: 0.84, 1.47 and 2.23. These large samples, selected with a uniform selection function, can be used to determine the $H\alpha$ luminosity function (LF) at each epoch, investigate any strong changes in its shape, and provide the first reliable estimate of the change in the global star-formation rate of the Universe between $z = 0$ and 2.2 using a single tracer of star-formation.

It is not only the global average star-formation rate which is important for our understanding of galaxy formation and evolution, but more crucially the nature and distribution of the star-forming galaxies at high redshifts. Galaxies form and evolve within the hierarchically growing dark-matter haloes of a Λ -CDM Universe, but the details of the galaxy formation process depend upon the complicated gas dynamics of star formation and feedback, and these processes are poorly understood. A surprising result of many recent studies is that the stellar populations of the most massive galaxies formed earlier than those of less massive galaxies – a process often referred to as “downsizing” (e.g. Cowie et al. 1996). Massive galaxies must therefore form stars rapidly at an early epoch, and then have their star-formation truncated, for example by feedback from AGN (e.g. Bower et al. 2006; Best et al. 2006) – but the epoch at which this occurred is still uncertain. In the local Universe, star-formation is also suppressed in dense environments (e.g. Lewis et al. 2002, Best 2004); this effect diminishes with increasing redshift, with hints that it disappears altogether at $z \sim 2$ (Kodama et al. 2007). But where precisely, in terms of epoch and environment, does this environmental influence begin to become important, and to what extent is the build-up of galaxies into groups and clusters since $z \sim 1$ responsible for the sharp decline of the cosmic star-formation rate density since $z \sim 1$?

HiZELS aims to tackle all of these issues by obtaining large samples of star-forming galaxies in representative volumes at three epochs across the peak epoch of star-formation in the Universe. Coupled with lower redshift studies, we are determining how the stellar mass of $H\alpha$ -selected galaxies declines with redshift between $z = 2.2$ and $z = 0$, investigating the physical processes involved in the downsizing activity. We are investigating changes in the $H\alpha$ luminosity function as a function of environment at each epoch and between different epochs: sky areas of a few square degrees are required to probe the full range of galaxy environments at these redshifts. The samples are also large enough to give a robust measurement of the clustering properties of sub-populations of the $H\alpha$ emitters, split by other properties like mass or star-formation rate; this provides important insights into their properties, including information about the relative masses of their dark matter haloes. Combining all of this information, HiZELS will provide a strong test of theoretical models of galaxy evolution (e.g. Benson et al. 2000; Baugh et al. 2005; Bower et al. 2006) and a direct input into these models.

In these proceedings we outline the current status and future plans of HiZELS. In Section 2, we describe the observational strategy. In Section 3, we show the constraints obtained on the $H\alpha$ luminosity function and cosmic star-formation rate, and discuss the other scientific results to date. We outline our on-going scientific work using HiZELS, and discuss future plans, in Section 4. Section 5 presents brief conclusions.

2. Observations and sample selection

2.1 Observation strategy and fields

HiZELS uses observations through narrow-band filters in the J , H and K -bands (NB_J , NB_H , $H_2(S1)$,

with central wavelengths of 1.211, 1.619 and 2.121 μm respectively), using WFCAM on UKIRT. Coupled with broad-band filter observations, these are used to detect star-forming galaxies in $\text{H}\alpha$ at redshifts 0.84, 1.47 and 2.23, over several degree-scale regions of the extra-galactic sky. Of course, narrow-band surveys are not sensitive to only one emission line, but will detect many different emission lines at different redshifts, redshifted into the filter. To achieve many of our goals it is necessary to identify which of the emission-line objects are indeed $\text{H}\alpha$ emitters. HiZELS is achieving this by targeting the best-studied regions of the extragalactic sky, in which a wealth of multi-wavelength data already exists. Photometric redshifts and colour-selections are being backed up by statistical analysis of the contamination rates derived from follow-up spectroscopy of sub-samples of emitters, as described below.

The presence of other emission line samples within the filters is actually one of the strengths of HiZELS. The custom-made NB_H and NB_J filters were specially designed such that the [OIII] 5007 and [OII] 3727 lines would fall into those filters for galaxies at $z = 2.23$. This provides both a confirmation of the redshifts for a subset of the $z = 2.23$ $\text{H}\alpha$ -selected sample, as well as allowing a first investigation of the emission line properties of these sources. Other emission lines of interest for these filters include the possibility of detecting $\text{Ly}\alpha$ emission from galaxies at $z = 8.90$ in the NB_J filter.

HiZELS was awarded 22 nights on UKIRT over Semesters 07B to 09B for its first phase (of which roughly one-third has been lost to bad weather), and has a provisional allocation of 23 clear nights for a second phase, during semesters 10A to 12A (subject to UKIRT remaining operational). The original survey strategy involved observations of each field in each of the three filters for a total on-sky observing time of ≈ 20 ks/pix, in order to obtain uniform coverage down to a line flux of 10^{-16} $\text{erg s}^{-1}\text{cm}^{-2}$ in each filter. In addition, a single deeper paw-print (ie. 0.2 sq. deg., to 65ks/pix depth) using the $\text{H}_2(\text{S1})$ filter has been taken to probe further down the $\text{H}\alpha$ luminosity function and assess the completeness of the shallower but wider survey. As the survey has progressed, the observing strategy has been slightly modified based on the survey results, to an overall aim of observing as close as possible to 1000 $\text{H}\alpha$ emitters at each redshift, split roughly half-and-half above and below the break of the luminosity function at each redshift. To achieve this, additional deeper paw-print observations are proposed using the $\text{H}_2(\text{S1})$ and NB_H filters, whilst the depth of the standard survey observations using the NB_J and NB_H filters, beyond the first two fields, has been reduced. The full set of proposed observations for HiZELS, along with the current observation status, is provided in Table 1.

Table 1: the HiZELS target fields, proposed exposure times, and current observational status.

Field Name	Area [sq. deg.]	Target exposure time (ks/pix)			Completion (% , Dec 2009)		
		NB_J	NB_H	$\text{H}_2(\text{S1})$	NB_J	NB_H	$\text{H}_2(\text{S1})$
UKIDSS UDS	0.8	20.0	20.0	20.0	100%	100%	100%
COSMOS-1*	0.8	20.0	20.0	20.0	100%	50%	100%
COSMOS-2*	0.8	3.0	14.0	20.0	0%	0%	0%
ELAIS N1	0.8	3.0	14.0	20.0	0%	38%	100%
SA 22	0.8	3.0	14.0	20.0	0%	0%	50%
Boötes	0.8	3.0	14.0	20.0	0%	0%	0%
Lockman Hole	0.8	3.0	14.0	20.0	0%	0%	0%
COSMOS-DeepK	0.4			65.0			50%
COSMOS-DeepH	0.2		50.0			0%	

* – two WFCAM pointings will be placed inside the 2 sq. deg. COSMOS field.

2.2 Selection of narrow-band $\text{H}\alpha$ emitters

Combining the narrow-band observations with broad-band observations of the same fields (either our own dedicated observations, or archival data from the UKIDSS survey), narrow-band emitters are selected according to the following criteria: (i) the object must be robustly detected on the narrow-band image, with a signal-to-noise (S/N) above 3, in a 3-arcsec diameter aperture; (ii) it must present a ‘broad-band minus narrow-band’ colour excess with a significance $\Sigma \geq 2.5$; (iii) the line emission must have

equivalent width above 50\AA ; (iv) the object must be visually confirmed as reliable, and not associated with any cross-talk artefact. The left panel of Figure 1 shows these selection criteria for the NB_J observations of the COSMOS-1 pointing. For more details on these selections, see Geach et al. (2008; hereafter G08) or Sobral et al (2009a; hereafter S09a). S09a have shown that these criteria are very robust.

Our observations identify approximately 800, 350 and 300 narrow-band emitters per pointing (0.8 sq. deg.) in the NB_J , NB_H , and $\text{H}_2(\text{S1})$ observations, respectively. Photometric redshifts and colour selections are then used to identify which of the emission line galaxies are $\text{H}\alpha$. We are able to successfully recover relatively clean $\text{H}\alpha$ samples, since strong contaminating emission lines are sufficiently well spread in wavelength from $\text{H}\alpha$ that photometric redshifts do not have to be very precise: $\delta z/z \sim 0.5$ – more details can be found in G08, S09a, Sobral et al. (2010c), and Geach et al. (2010). In the NB_J observations, photometric redshifts indicate that over half of the detected emitters are indeed $\text{H}\alpha$ emitters at $z = 0.84$, with a significant fraction of the remainder being $\text{H}\beta$ or $[\text{OIII}]$ emitters at $z \sim 1.4$ (see middle panel of Figure 1). Archival spectroscopic redshifts for over 100 of the emitters confirm the high completeness and reliability of the photometric selection (Figure 1, right panel; see also S09a). In the COSMOS and UDS fields, photometric redshifts provide a similar level of accuracy for selecting $\text{H}\alpha$ emitters at $z = 1.47$ from the NB_H observations (see Sobral et al. 2010c), and approximately half of the narrow-band emitters are associated with $\text{H}\alpha$. The $\text{H}_2(\text{S1})$ observations suffer considerably more contamination from lower redshift emitters (e.g. Paschen and Brackett series; see G08), but are producing around 90 candidate $z = 2.23$ sources per field.

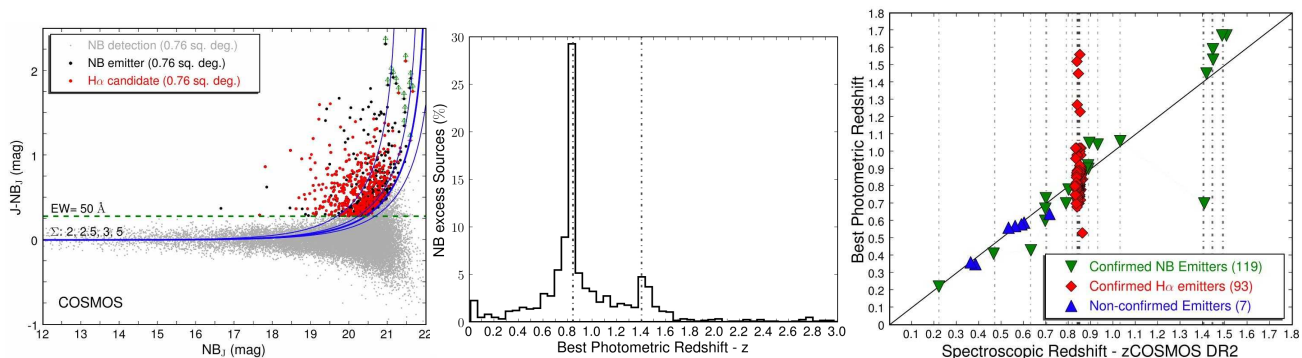


Fig. 1. Left: A colour-magnitude plot demonstrating the selection of narrow-band excess sources (adopted from S09a). All $> 3\text{-}\sigma$ detections in the NB_J image are plotted and the curves represent Σ significances of 5, 3, 2.5 and 2, respectively. The dashed line represents an equivalent width cut of 50\AA . All selected narrow-band emitters are plotted in black, while candidate $\text{H}\alpha$ emitters (selected using photometric redshifts) are plotted in red. Middle: The distribution of photometric redshifts of the NB_J excess sources, showing clear peaks for $\text{H}\alpha$ at $z = 0.84$ and $\text{H}\beta$ or $[\text{OIII}]$ at $z \sim 1.4$. Right: a comparison between photometric and archival spectroscopic redshifts, demonstrating the reliability of the sample.

3 Scientific results from HiZELS

3.1 The $\text{H}\alpha$ luminosity function and the cosmic star-formation rate density

HiZELS has already resulted in by far the largest and deepest survey of emission line selected star-forming galaxies at each of the three targeted redshifts, and has greatly improved determinations of the $\text{H}\alpha$ luminosity function. It has produced the first reliable $\text{H}\alpha$ LF at $z = 2.23$ (G08; Geach et al. 2010), as well as providing the first statistically significant samples at redshifts 0.84 (S09a) and 1.47 (Sobral et al. 2010c). The luminosity functions are derived after correcting the observations for: (i) contamination of the emission line flux by the nearby $[\text{NII}]$ line (using the relation between the flux ratio $f_{[\text{NII}]} / f_{\text{H}\alpha}$ and the total measured equivalent width; cf S09a); (ii) extinction of the $\text{H}\alpha$ emission line, taken to be the canonical value of 1 magnitude (but see Section 3.5 for more details on this); (iii) the detection completeness of faint galaxies, and the selection completeness for detected galaxies with faint emission lines (evaluated through Monte-Carlo simulations); (iv) filter profile effects, due to the filter not being a perfect top-hat (again, evaluated through Monte-Carlo simulations). For more details see G08 and S09a.

The derived luminosity functions show very strong evolution from redshift zero out to $z = 2.23$ (G08, S09a; left panel of Figure 2). At all redshifts the $H\alpha$ LF is found to be well-fitted by a Schechter function, but the form of the LF undergoes dramatic evolution through the redshift range probed by HiZELS. ϕ^* and L^* both evolve strongly from the local Universe out to $z \sim 1$, but beyond that L^* continues to rise up to $z \sim 2$ whilst ϕ^* peaks at $z \sim 1$ and then decreases at higher redshifts. The integrated luminosity function, corrected for AGN contamination, is used to estimate the cosmic star-formation rate density (ρ_{SFR}) at each redshift; using a single star-formation tracer ($H\alpha$) from $z = 0$ to $z = 2.23$, ρ_{SFR} is found to rise strongly up to $z \sim 1$ and then appears to flatten out to $z \sim 2.2$ (right panel of Figure 2).

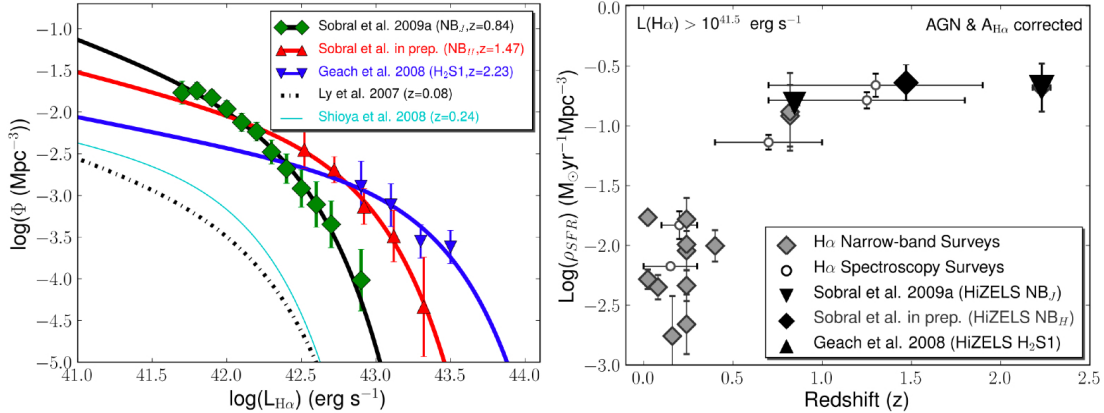


Fig. 2. *Left: the $z = 0.84$, $z = 1.47$ and $z = 2.23$ $H\alpha$ luminosity functions from HiZELS (corrected for $[NII]$ contamination, completeness, extinction and filter profile biases) with the best-fit Schechter functions overlaid. Other luminosity functions from $H\alpha$ surveys at different redshifts are presented for comparison, showing a clear evolution of the LF out to $z > 2$. Right: the evolution of ρ_{SFR} as a function of redshift based on $H\alpha$ (down to the HiZELS limit). This shows a rise in ρ_{SFR} up to at least $z \sim 1$, slightly steeper than the canonical $(1+z)^4$, followed by a flattening out to at least $z \sim 2.2$.*

3.2 The morphologies of the $H\alpha$ emitters

At $z = 0.84$, the $H\alpha$ emitters are mostly morphologically classed as disks, with irregulars and mergers forming a much smaller fraction of the sample (S09a). A strong relation is found between morphology and $H\alpha$ luminosity, however, with the fraction of irregulars/mergers rising steadily with luminosity and the fraction of quiescent disks falling; the break of the luminosity function seems to define a critical switch-over luminosity between the two populations. Out to $z \sim 1$, the integrated ρ_{SFR} is produced predominantly by disk galaxies and it is their evolution which drives the strong increase in the cosmic star-formation rate density from the current epoch to redshift one. In contrast, the continued strong evolution of L^* between $z = 0.84$ and $z = 2.23$ suggests an increasing importance of merger-driven star-formation activity beyond $z \sim 1$, as mergers and irregulars dominate the bright end of the luminosity function. Analysis of the first $z = 2.23$ $H\alpha$ emitters (G08) indicates that these do show a range of morphologies, and that indeed many show evidence of on-going merger activity. The completed HiZELS survey will provide statistically significant samples of $H\alpha$ emitters at $z = 2.23$ and $z = 1.47$, allowing a direct test of whether the change in the form of the luminosity function at $z \sim 1$ is driven by the different evolutionary behaviour of these two different populations of star-forming galaxies.

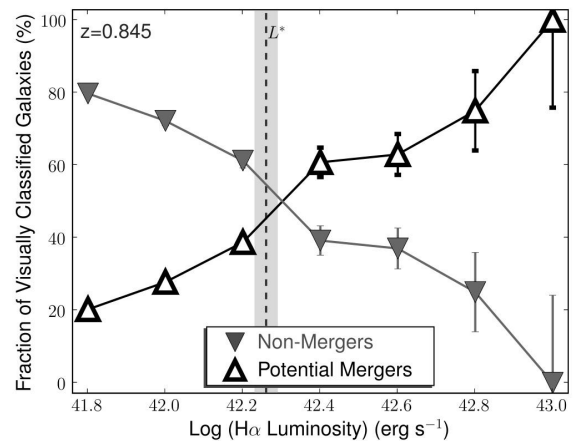


Fig. 3. *The merger fraction as a function of $H\alpha$ luminosity at $z = 0.84$. This shows a clear dependency, with mergers dominating above L^* and passive quiescent galaxies dominating below that.*

3.3 Clustering of star-forming galaxies and environmental variations

HiZELS is ideal for investigating the clustering of SF galaxies because the narrow-band selection removes almost all of the projection effects which usually degrade clustering analysis based on imaging data. The HiZELS emitters are observed to be significantly clustered at all redshifts. At $z = 0.84$ the characteristic correlation length calculated from the $H\alpha$ emitters is $r_0 = 2.7 \pm 0.3 h^{-1}$ Mpc (Sobral et al. 2010a), consistent with them residing in dark matter halos of mass $\sim 10^{12} M_\odot$ at that epoch, close to that expected for the progenitors of galaxies like the Milky Way. Using the large sample available at this redshift, the clustering is found to be strongly dependent on $H\alpha$ luminosity, and also to increase more weakly with near-infrared luminosity (roughly tracing stellar mass). The clustering amplitude is found to be independent of morphology, once the dependencies of morphology on stellar mass and star-formation rate have been accounted for. These results, shown in Figure 4, are qualitatively in line with those found in the nearby Universe.

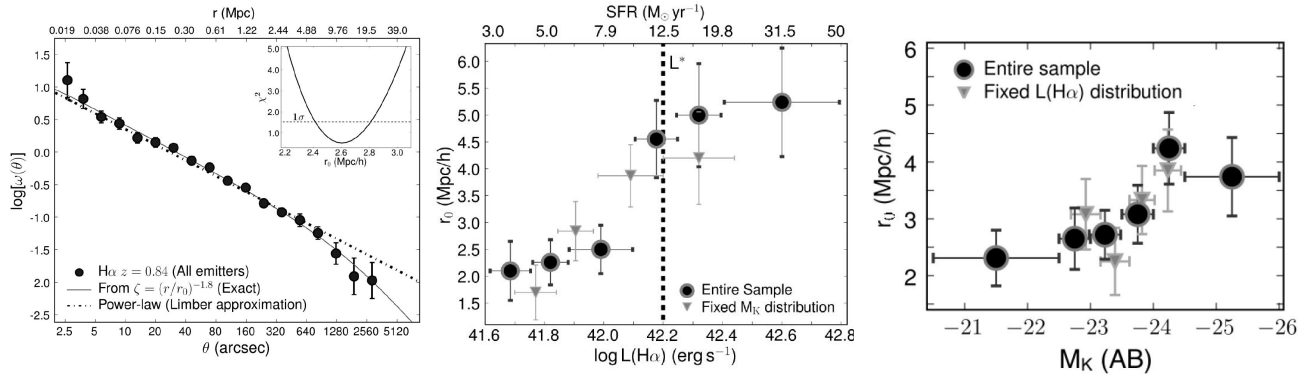


Fig. 4. Left: the angular cross-correlation function of $H\alpha$ emitters at redshift $z = 0.84$ in the COSMOS and UDS fields. Middle, right: the dependence of the clustering amplitude at this redshift on star-formation rate and absolute K -band magnitude.

The left-panel of Figure 5 shows the clustering amplitude of $H\alpha$ emitters measured from narrow-band surveys at different redshifts. However, the strong dependence of the clustering amplitude on $H\alpha$ luminosity implies that considerable care must be taken when attempting to compare these, since they have very different luminosity limits. The right-hand panel of Figure 5 compares the clustering amplitude of the $H\alpha$ emitters, as a function of $H\alpha$ luminosity, at three different redshifts: $z = 0.84$ and $z = 2.23$ from HiZELS (Sobral et al. 2010a, and G08), and $z = 0.24$ from Shioya et al. (2008). It can be seen that at a given halo mass, star-formation is much more efficient (higher $L_{H\alpha}$) at higher redshifts.

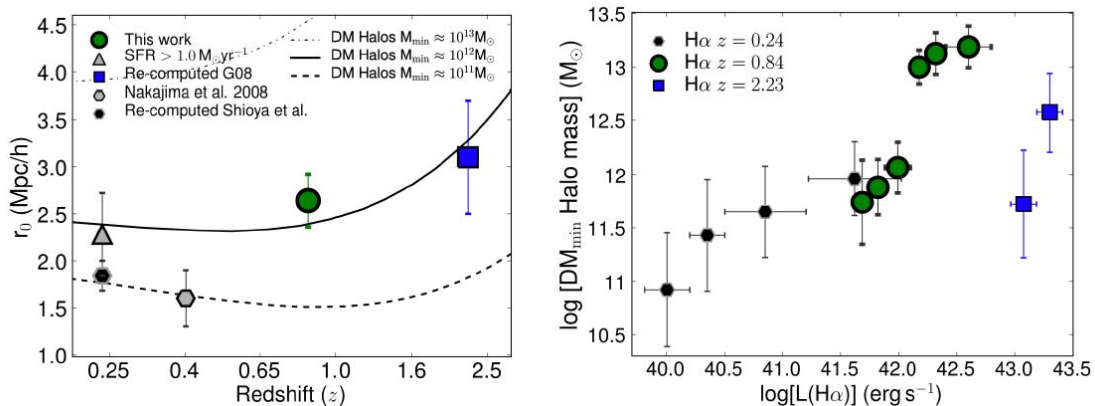


Fig. 5. Left: The clustering length (r_0) as a function of redshift for $H\alpha$ emitters selected by narrow-band surveys. The $H\alpha$ emitters at $z = 0.84$ and $z = 2.23$ studied by HiZELS reside in typical dark matter haloes of $M_{\min} \approx 10^{12} M_\odot$, consistent with being the progenitors of Milky-Way type galaxies. The lower luminosity $H\alpha$ emitters found in smaller volumes at $z = 0.24$ and $z = 0.4$ reside in less massive haloes. Right: The minimum mass of host dark matter haloes as a function of $H\alpha$ luminosity at three different redshifts. From Sobral et al. (2010a).

The increase in $L_{H\alpha}$ at given halo mass with redshift nearly exactly mirrors that of the increase in L^* of the $H\alpha$ luminosity function. This implies that galaxies in a given dark matter halo mass may form stars at the same fraction of the characteristic star-formation rate at that redshift, at all epochs (cf. Sobral et al. 2010a). This in turn would suggest a fundamental connection between the strong negative evolution of the $H\alpha L^*$ since $z \sim 2$ and the quenching of star-formation in galaxies within haloes significantly more massive than $10^{12} M_{\odot}$.

3.4 The masses and environments of star-forming galaxies

In the nearby Universe, the stellar populations of the most massive galaxies are observed to have formed earlier than those of less massive galaxies. The HiZELS sample allows a direct investigation of the redshift at which this “down-sizing” process began, and a measurement of how the characteristic stellar mass of star-forming galaxies varies with redshift. At $z = 0.84$ we find a strong dependence of the proportion of galaxies which are actively forming stars as a function of mass: for $M \approx 10^{10} M_{\odot}$, around a third of galaxies are detected by HiZELS, but at higher masses ($> 10^{11.5} M_{\odot}$) this fraction falls away to a value consistent with zero (Sobral et al. 2010b). This indicates that down-sizing is already in place at $z = 0.84$.

We find that at $z = 0.84$ the fraction of star-forming galaxies increases with local galaxy surface density at low galaxy surface densities, but then falls in group and cluster environments (Figure 6). The median star formation rate of the $H\alpha$ emitters increases with local galaxy density: those residing in denser regions are mostly starbursts while the $H\alpha$ emitters found in less dense regions present much more quiescent star-formation. Our results resolve the apparent contradictions between different studies presented in the literature, which have found the star-forming galaxy fraction to increase (e.g. Elbaz et al 2007, studying field galaxies) or decrease (e.g. Patel et al 2009, studying galaxies in the high density regions around a rich cluster) with increasing environmental density: both trends exist, and which is observed depends upon the range of environmental densities studied.

With the full HiZELS sample we will be able to investigate how these relations with mass and environment evolve to higher redshifts, over 80% of the lifetime of the Universe

3.5 The dust extinction properties of high- z star-forming galaxies

Deep $24\text{-}\mu\text{m}$ data from *Spitzer* are available in most of the HiZELS fields, and 35% of the $z = 0.84$ HiZELS $H\alpha$ emitters in UDS and COSMOS are detected at $24\mu\text{m}$. Using these detections and stacking analyses, the star-formation rate estimates from the HiZELS $H\alpha$ sample can be compared with those from the mid-infrared to estimate the dust extinction properties of the star-forming galaxies. We find a clear trend for an increase in mean dust extinction with increasing star formation rate at $z = 0.84$ (Garn et al. 2009; see Figure 7). The relation we determine broadly matches that found in the low redshift Universe by Hopkins et al. (2001), suggesting that there is no significant change in the dust properties of star-forming galaxies with redshift, at least out to $z \sim 1$. We find no variation of the extinction–SFR relation with galaxy morphology, environment or merger status. Carrying out equivalent analyses at the higher HiZELS redshifts will be a key goal when the samples are sufficiently large.

We are exploiting the exquisite multi-wavelength data available for our fields to understand the spectral energy distribution of typical star-forming galaxies across a range of redshifts. We aim to compare

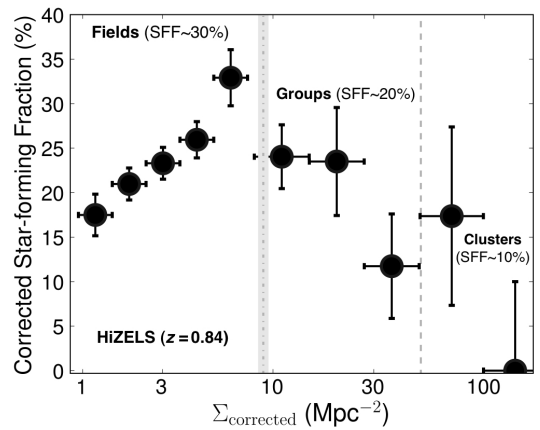


Fig. 6. The fraction of galaxies forming stars as a function of local galaxy surface density, for $H\alpha$ emitters at $z = 0.84$. The star-forming fraction increases with local surface density in the field, but then decreases in group and cluster environments.

additional star-formation tracers (UV continuum, [OII], sub-mm, radio) with our $H\alpha$ measurements.

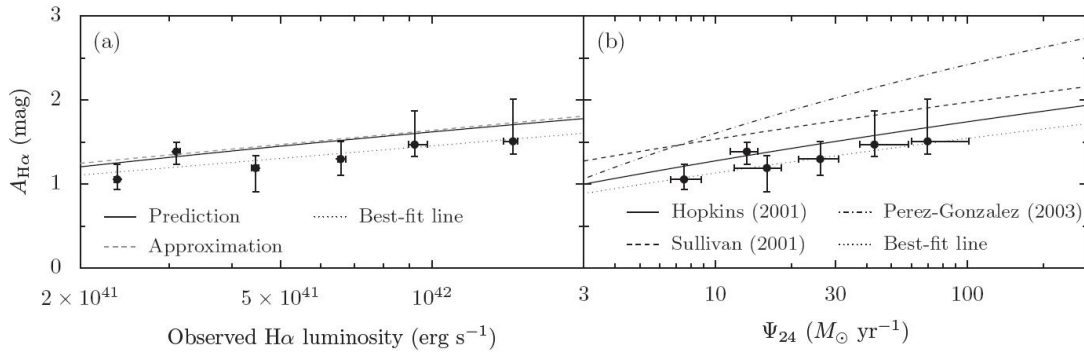


Fig. 7. The variation in $H\alpha$ extinction for $H\alpha$ emitters binned by their observed $H\alpha$ flux, as a function of $H\alpha$ luminosity (left) or $24\mu\text{m}$ star-formation rate (right). The best-fit (dotted line) shows that, at the 4σ confidence level, extinction increases with star-formation rate. The slope and normalisation of the relationship are comparable to those derived in the local Universe using the fit between the Balmer decrement and SFR, by Hopkins et al. (2001).

3.6 Limits on the space density of bright $z = 8.9$ $\text{Ly}\alpha$ emitters

Parallel to our $H\alpha$ survey using the NB_J filter, we have explored its capabilities to detect bright $\text{Ly}\alpha$ emitters at $z = 8.9$, when the Universe was only ~ 0.5 Gyr old. Detection of any such objects would have important consequences for our understanding of the early star-formation history of the Universe, as well as providing an important probe of the re-ionisation of the Universe. After conducting an exhaustive search for such emitters in the UDS and COSMOS fields, two candidates were isolated, both in the COSMOS field. Follow-up spectroscopy using CGS4 in January 2009, together with follow-up J -band imaging obtained in February 2009 with WFCAM has shown that these cannot be $\text{Ly}\alpha$ emitters. These results have allowed us to improve constraints on the bright end of the $z \sim 9$ $\text{Ly}\alpha$ luminosity function by three orders of magnitude (Sobral et al. 2009b).

4. On-going work and future plans

HiZELS offers a powerful resource for a large number of additional studies. Other on-going work includes the following:

- *Spectroscopic confirmation of emission lines and study of emission line ratios.* We have followed-up HiZELS $\text{H}_2(\text{S}1)$ $H\alpha$ emitters using near-infrared spectroscopic observations, both with VLT/ISAAC and with Gemini. These observations have successfully confirmed the HiZELS emission line detections, and the results will be published in Geach et al. (2010). We are carrying out optical spectroscopic observations of a large fraction of the emitters selected from all 3 narrow bands (NB_J , NB_H & $\text{H}_2(\text{S}1)$), in the UDS field, using VIMOS. The main aims are to confirm redshifts, to investigate line-ratios and extinction, to identify AGN, and to test the robustness of the selection criteria used for HiZELS. By allowing pre-selection of galaxies with known emission lines in the J - and H -bands, HiZELS will also provide a valuable input sample for early commissioning tests for FMOS, the new near-IR multi-object spectroscope on Subaru; such observations will allow us to confirm emission lines, redshifts, identify AGN, and study sample contaminants.
- *Complementary narrow-band observations.* Using HAWK-I on VLT we have carried out ultra-deep $\text{H}_2(\text{S}1)$ exposures in two small regions in the COSMOS and UDS fields. These will reach a depth of $\approx 3M_\odot\text{yr}^{-1}$ at $z = 2.23$, comparable to the HiZELS NB_J sensitivity, and will thus provide an excellent complement to our shallower but much wider HiZELS imaging. This will enable an accurate measurement of the very faint end of the $H\alpha$ luminosity function at $z \sim 2.23$, determining the global star-formation history and testing for differential evolution of the most/least active galaxies.

- *Ly α and H α emission from galaxies at $z = 2.23$.* We are exploiting existing narrow-band Ly α imaging of the COSMOS field from Nilsson et al. (2009) to compare the Ly α and H α properties of galaxies at $z = 2.23$. Ly α emission has been extensively used to identify and study large samples of star-forming galaxies at the highest redshifts, but its reliability as a tracer of complete galaxy populations remains untested at cosmological distances. By combining our H α sample with Ly α observations we can derive the ratio of Ly α to H α emission and hence obtain a direct measurement of the escape fraction of Ly α photons with few model assumptions – something which has never been done at high redshift. We find that only a modest fraction, $10 \pm 3\%$, of H α emitters are detected in Ly α above a rest-frame equivalent width of 20\AA (Matsuda et al. 2010, in prep). This detection rate is similar to that seen for $z \sim 2.3$ UV-continuum selected galaxies (Reddy et al. 2009) and is less than that seen for $z \sim 3$ Lyman-break galaxies (Shapley et al. 2004). Stacking the H α sources we find potential evidence for extended Ly α halos, similar to that seen around $z \sim 3$ LBGs by Hayashino et al. (2004).
- *Paschen-series luminosity functions.* In our H $_2$ (S1) imaging we are also detecting large samples of Pa α , Pa β and other lines from lower redshift sources. Whilst our photometric selection is very efficient at filtering out these contaminants from our H α studies, we aim to present a robust analysis of the extent and character of the contamination. This may allow the derivation of Pa-series galaxy luminosity functions, which would provide a new measure of the cosmic star-formation rate density, and an estimate of extinction.
- *Kinematics of HiZELS galaxies.* We are using the SINFONI near-IR integral field spectrograph on VLT to map the kinematics of the H α emission in a sample of 18 H α emitters at $z = 0.84$, $z = 1.47$ and $z = 2.23$ in the COSMOS field. This project exploits HiZELS panoramic coverage to select sources at each redshift which are matched on H α -luminosity and, critically, are close to natural AO guide stars. These observations will allow us to map the distribution of H α emission on $\sim 0.2''$ scales within these galaxies to search for kinematic evidence of rotating discs, major mergers, etc. This detailed follow-up will be a valuable addition to HiZELS, allowing us to study the properties of the progenitors of Milky Way-type galaxies seen at the time when their star-formation was at its peak.
- *Comparison with galaxy formation models.* HiZELS provides a large sample of star-forming galaxies at three different redshifts, the selection of which can be cleanly replicated in (and compared with) theoretical semi-analytic models of galaxy formation. An initial comparison of the luminosity function and clustering properties of the H α emitters at $z = 2.23$ was presented in G08, showing that these were broadly in line with those predicted by one particular “recipe” of galaxy formation, that of Bower et al. (2006). Now with larger datasets available at all three wavelengths, far more detailed investigations are beginning, folding in the variations of the luminosity function and clustering of the HiZELS galaxies with morphology, mass, etc. These studies will offer an invaluable ingredient to these models.

5. Conclusions

The advent of wide-field imaging cameras in the near-IR, especially WFCAM on UKIRT, has revolutionised the study of high-redshift emission line galaxies. HiZELS aims to detect and study up to a thousand H α emitting galaxies at each of three redshifts, 0.84, 1.47 and 2.23, spanning the peak epoch of star-formation in the Universe. This goal is already nearly completed at $z = 0.84$, and has resulted in a plethora of results related to the luminosity function, masses, morphologies, environments, clustering, dust extinction, and other properties of the star-forming galaxies at this redshift. Results at the higher redshifts remain sparser to date, because the current samples are smaller due to the lower sky density of H α emitters at these higher redshifts: as the survey progresses, we will replicate our $z = 0.84$ studies at the higher redshifts, where arguably our H α studies will be most unique, and the impact of HiZELS will be highest.

Acknowledgements

HiZELS is based on observations obtained with the Wide Field CAMera (WFCAM) on the United Kingdom Infrared Telescope (UKIRT). We are indebted to Andy Adamson, Luca Rizzi, Chris Davis, Tim, Thor and Jack for their support at the telescope. PNB is grateful for support from the Leverhulme Trust, DS for support from the FCT, and JEG for support from STFC.

This article is dedicated to the memory of Timothy Garn, a valued member of the HiZELS team, whose nature has cruelly taken away at a time when the prime of his research career was still in front of him.

References

- Baugh C.M. et al. 2005, MNRAS, 356, 1191
Benson A.J., Cole S., Frenk C.S., Baugh C.M., Lacey C.G., 2000, MNRAS, 311, 793
Best P.N., 2004, MNRAS, 351, 70
Best P.N., Kaiser C.R., Heckman T.M., Kauffmann G., 2006, MNRAS, 368, L67
Bower R. et al. 2006, MNRAS, 370, 645
Cowie L.L., Songaila A., Hu E.M., Cohen J.G., 1996, AJ, 112, 839
Doherty M., Bunker A., Sharp R., Dalton G., Parry I., Lewis I., 2006, MNRAS, 370, 331
Elbaz D. et al., 2007, A&A, 468, 33
Gallego J., Zamorano J., Aragon-Salamanca A., Rego M., 1995, ApJL, 455, L1
Garn T. et al. 2009, MNRAS, in press, arXiv/0911.2511
Geach J.E., Smail I., Best P.N., Kurk J., Casali M., Ivison R.J., Coppin K., 2008, MNRAS, 388, 1473
Geach J. et al. 2010, MNRAS, in prep.
Hayashino T. et al. 2004, AJ, 128, 2073
Hopkins A. M., Beacom J. F., 2006, ApJ, 651, 142
Ivison R. et al. 2007, MNRAS, 380, 199
Kennicutt R.C. Jr, 1998, ARAA, 36, 189
Kodama T. et al. 2007, MNRAS, 377, 1717
Lewis I. et al. 2002, MNRAS, 334, 673
Lilly S.J., Le Fevre O., Hammer F., Crampton D., 1996, ApJL, 460, L1+
Moorwood A.F.M., van der Werf P.P., Cuby J.-G., Oliva E., 2000, A&A, 326, 9
Moustakas J., Kennicutt R.C. Jr., Tremonti C.A., 2006, ApJ, 642, 775
Nilsson K.K. et al. 2009, A&A, 498, 13
Patel S.G., Holden B.P., Kelson D.D., Illingworth G.D., Franx M., 2009, ApJ, 705, L67
Reddy N.A., Steidel C.C., 2009, ApJ, 692, 778
Shapley A.E., Erb D.K., Pettini M., Steidel C.C., Adelberger K.L., 2004, ApJ, 612, 108
Shioya Y. et al. 2008, ApJS, 175, 128
Sobral D. et al., 2009a, MNRAS, 398, 75
Sobral D. et al., 2009b, MNRAS, 398, L68
Sobral D., Best P.N., Geach J.E., Smail I., Cirasuolo M., Garn T., Dalton G.B., Kurk J., 2010a, MNRAS, in press, arXiv/0912.3888
Sobral D., Best P., Geach J., Smail I., Cirasuolo M., Garn T., Kurk J., Dalton G., 2010b, MNRAS, submitted
Sobral D. et al. 2010c, MNRAS, in prep
Tresse L., Maddox S.J., Le Fevre O., Cuby J.-G., 2002, MNRAS, 337, 369
Yan L., McCarthy P.J., Freudling W., Teplitz H.I., Malumuth E.M., Weymann R.J., Malkan M.A., 1999, ApJL, 519, L47